Photoisomerization-Controlled Phase Segregation in a Submicron Confined Azonematic Liquid Crystal

B. Zupančič,[1,2,3] S. Diez-Berart,[4] D. Finotello,[5] O. D. Lavrentovich,[6] and B. Zalar[1,2,3]

[1]*Jožef Stefan Institute, Jamova cesta 39, SI-1000 Ljubljana, Slovenia*
[2]*Centre of Excellence NAMASTE, Jamova cesta 39, SI-1000 Ljubljana, Slovenia*
[3]*Centre of Excellence EN-FIST, Dunajska cesta 156, SI-1000 Ljubljana, Slovenia*
[4]*Grup de les Propietats Físiques dels Materials (GRPFM), Departament de Física i Enginyeria Nuclear, E.T.S.E.I.B., Universitat Politècnica de Catalunya, Barcelona, Spain*
[5]*National Science Foundation, 4201 Wilson Blvd., Arlington, Virginia 22230, USA*
[6]*Liquid Crystal Institute, Kent State University, Kent, Ohio 44242-0001, USA*

(Received 29 March 2012; published 18 June 2012)

Deuteron nuclear magnetic resonance is used to study the phase segregation behavior of photoisomerizable liquid crystal diheptylazobenzene (7AB) confined into cylindrical pores of Anopore membranes. It is demonstrated that the concentration of both components in a binary *trans*-7AB and *cis*-7AB mixture can be controlled dynamically using UV-illumination stimulated *trans*-to-*cis* photoisomerization and thermally induced *cis*-to-*trans* backisomerization. The so far elusive temperature-concentration phase diagram of such system is determined by comparative analysis of the behavior in bulk, thin-planar, and Anopore-confining geometry.

DOI: 10.1103/PhysRevLett.108.257801 PACS numbers: 61.30.Pq

In contrast to bulk states, liquid crystalline phases in restricted geometries are strongly affected by confining interfaces [1]. Pretransitional effects [2] and the promotion of supercritical behavior [3,4] are among the most interesting consequences of confinement in various geometries including ultrathin flat cells, cylindrical cavities, square capillary tubes, and random porous networks [3,5–7]. Photoisomerizable materials have often been employed to exploit the bulk-surface interplay, e.g., to induce isothermal phase transitions [8] or to create molecular traps by spatially modifying liquid crystalline order [9]. In most experimental and theoretical studies, the confined mesogen is assumed to be pure, i.e., single-component, allowing for the possible component- and phase-segregation tendencies, characteristic of multicomponent systems, to be disregarded. Recently, however, photochemical phase transition and thermochromic behavior were shown to be altered considerably, as compared to the homopolymer case, in microphase-separated domains of azobenzene-containing diblock copolymers [10]. This observation raises a related question on how to describe the surface-controlled pretransitional behavior of multicomponent vs single-component liquid crystal, confined to a solid matrix. Specifically, what are the implications of demixing of components and the resulting isotropic (I)—nematic (N) phase coexistence, encountered in bulk multicomponent systems [11], for the surface-induced paranematic (PN) phases [12,13] present in restricted geometries? Confining a binary mixture to a controlled pore geometry solid substrate [1] would seem to be an obvious choice to address the above question. Unfortunately, in order to experimentally investigate the temperature-concentration (T-ϕ) phase diagram, a rather tedious preparation of numerous samples of different ϕ is required. Moreover, predefined and unalterable ϕ in a particular sample prevents a successful implementation for applications of physical properties specific of multicomponent systems, such as (i) change in the N-I phase transition temperature T_{NI} on varying ϕ, (ii) broad, ϕ-dependent N-I temperature coexistence range, and (iii) possible ϕ-controlled pretransitional ordering at the confining surfaces. Due to the lack of a realistic model system not subject to the above restriction, the interplay between multicomponent composition and surface-controlled paranematic ordering has hardly been discussed so far, let alone been well understood.

In this Letter, we present a novel method for experimental and theoretical description of binary confined liquid crystal systems, which allows us to characterize efficiently the T-ϕ phase diagram of the low-temperature nematic order parameter S and high-temperature, surface interactions-controlled averaged paranematic order parameter $\overline{S(r)}$. We demonstrate that confined photoisomerizable mesogenic dye can be considered as a model binary confined liquid crystal with "adjustable" ϕ. *Trans* and *cis* isomers represent the two components, the concentrations of which can easily be controlled by illumination time-profile. This lift of restriction of constant ϕ provides for experimental access to an arbitrary point in the T-ϕ phase diagram within a single specimen. We use quadrupole-perturbed deuteron NMR (DNMR) as an experimental tool, as well as phenomenological Landau–de Gennes (LdG) free energy modeling, extended with ϕ-dependent surface interaction terms, to determine this phase diagram.

Liquid crystal material used in the study was diheptylazobenzene (7AB) [14], which exhibits a nematic phase between 313.2 K and 320.2 K at ambient room light conditions. The material, deuterium labeled at the α-position of the hydrocarbon chain, was confined to 60-μm-thick alumina membrane (Anopore) with cylindrical pores of $2R = 0.2$ μm in diameter. The membrane was subsequently trimmed to a 4×5 mm platelet and sealed into a flat glass cell using a standard two-component epoxy (the sample henceforth referred to as "confined"). We also prepared a planar cell of about 55-μm thickness ("planar sample") and a cylindrical glass tube of 3-mm inner diameter filled with 1-cm-high column of 7AB ("bulk sample"). DNMR experiments were performed at the Larmor frequency $\nu_L(^2\mathrm{H}) = 58.337$ MHz, using phase-cycled solid echo pulse sequence $(90^\circ_x - \tau - 90^\circ_y - \tau)$ with 90° pulse width of 5 μs, $\tau = 50$ μs, and signal averaging repetition time of ≈ 100 ms. A home-built NMR probe head was equipped with an irradiation-detection coil, which allowed for uniform illumination of planar samples, with normal incidence, via quartz optical fiber. The output of the fiber was additionally collimated so that the irradiance variation across the incidence surface was less than 10%. In this way, uniform concentration $\phi = N_{cis}/(N_{cis} + N_{trans})$ of *cis* moieties was achieved in the sample. The output of an Oriel mercury short-arc lamp light source was filtered using a heat absorbing glass and a bandpass filter to limit the wavelength output to the 350–400 nm range covering the lamp's emission peak at $\lambda \approx 365$ nm, resulting in an efficient 7AB *trans* to *cis* isomerization. In order to create a uniform depth-profile of ϕ, planar and confined samples were illuminated *in situ* for at least 5 hours, during which molecular diffusion contributed to establishing a photostationary composition $\phi_0 = \phi(t=0)$ with strongly prevalent *cis*-population. Light was then switched off at $t = 0$ and DNMR spectra taken at successive time points t_n by averaging the signal over regular time intervals $\Delta t = t_{n+1} - t_n \approx 15$ min at a constant temperature. The Δt was kept much shorter than the backisomerization time scale τ (a few minutes vs several hours) so that, effectively, individual measurements at t_n were recorded in a dynamical equilibrium regime, i.e., at a constant ϕ. Measurements were repeated at several temperatures. The recorded time dependencies exhibited neither wavelength nor bandpass filter width dependence in the 350–400 nm range, supporting a conjecture of *cis*-prevalent initial state, i.e., $\phi_0 \to 1$. Previous studies of azobenzene and 7AB photoisomerization have shown that ϕ_0 strongly depends on the wavelength, with maximal ϕ_0 of about 0.8 [15,16]. However, these measurements were performed in solutions and not in the mesophases of pure 7AB.

A representative t-dependence of the DNMR spectra recorded at $T = 310$ K is shown in Fig. 1. The spectra provide for a straightforward identification of the three characteristic regions of the phase diagram in terms of

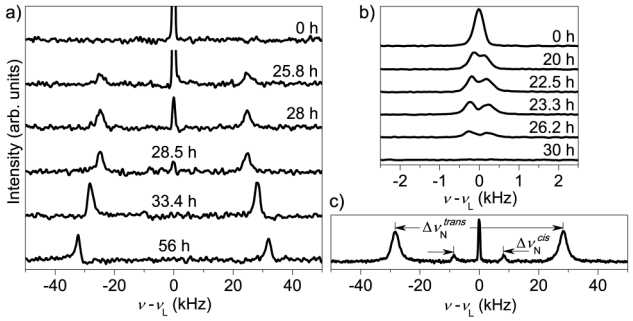

FIG. 1. (a) DNMR spectra of confined 7AB recorded at different times t during the thermal backisomerization process. The doublet with the splitting of about 65 kHz at $t = 56$ h and the central line detectable for t below 30 h arise from the N and PN phase, respectively. (b) Magnified view of the central line with resolvable paranematic splitting of about 1 kHz at $t = 25$ h. The sample was initially illuminated for 5 h with the temperature held constant at $T = 310$ K. (c) Extensive signal averaging reveals the presence of the second, inner doublet with a smaller splitting, attributed to *cis* isomers in the N phase.

increasing backisomerization time t: the paranematic (PN) phase at short t, the coexistence region of paranematic and nematic phases (N + PN) for intermediate t, and the nematic (N) phase in the long t limit when the equilibrium with all *trans* isomers is reestablished. PN phase is identified via the presence of the narrow and split central peak with integral intensity I_{PN}, reminiscent of the one commonly observed in confined systems with surface interactions [1], whereas N phase gives rise to the pair of doublets, the inner one of intensity I_{N}^{cis} originating from the *cis* and the outer one of intensity I_{N}^{trans} from the *trans* isomers. The backisomerization process, equivalently decreasing $\phi(t)$, is clearly reflected through the observed decay of I_{PN} and growth of $I_{\mathrm{N}} = I_{\mathrm{N}}^{cis} + I_{\mathrm{N}}^{trans}$ with increasing t. Let us note that the inner doublet of intensity I_{N}^{cis}, with approximately 1/3 frequency splitting of the outer doublet, can only be observed in the nematic phase when the S/N ratio is improved by averaging over longer time intervals [Fig. 1(c)]. *Cis* and *trans* isomers could not be resolved in the paranematic peak.

The frequency splitting of nematic doublet is proportional to the order parameter S and depends on the angle ϑ between the nematic director $\mathbf{n}$ and the external magnetic field $\mathbf{B_0}$, $\Delta\nu = \frac{3}{2}\bar{\nu}_Q S P_2(\cos\vartheta)$. The average quadrupolar frequency of α-deuterated 7AB, $\bar{\nu}_Q = 53$ kHz, was determined experimentally from a powder pattern of a frozen sample. In order to check for director configuration within the pores, we have also taken the angular-dependence spectra by varying the orientation of pore axes $\mathbf{a}$ with respect to $\mathbf{B_0}$. For both nematic and surface-induced doublet splittings, the angular patterns corresponded to axial ($\mathbf{n} \parallel \mathbf{a}$) director configuration [17]. Consequently, $\vartheta \angle(\mathbf{a}, \mathbf{B_0})$ was constant for all 7AB molecules at any orientation of the sample. All measurements used to

determine the phase diagram were performed at the orientation $\mathbf{a} \parallel \mathbf{B_0}$ so that $\Delta\nu_{\mathrm{PN}} = \frac{3}{2}\bar{\nu}_Q S_{\mathrm{PN}}$, $\Delta\nu_{\mathrm{N}}^{cis} = \frac{3}{2}\bar{\nu}_Q S_{\mathrm{N}}^{cis}$, and $\Delta\nu_{\mathrm{N}}^{trans} = \frac{3}{2}\bar{\nu}_Q S_{\mathrm{N}}^{trans}$, respectively for the three experimentally observed splittings. The T-ϕ phase diagram of the N-PN transition, i.e., relations $S_{\mathrm{PN}}(\phi)$, $S_{\mathrm{N}}^{cis}(\phi)$, and $S_{\mathrm{N}}^{trans}(\phi)$, can therefore be determined experimentally by relating S and ϕ via their t-dependencies during the backisomerization process. In contrast to $S(t)$, which is proportional to $\Delta\nu(t)$, $\phi(t)$ relates to DNMR spectrum in a more intricate way since, in order to reach the chemical equilibrium in the N + PN coexistence region, one has to allow for separation of components into a *cis*-rich PN phase and *cis*-poor N phase, equivalently $\phi_{\mathrm{N}} \leq \phi \leq \phi_{\mathrm{PN}}$. During the backisomerization, an exponential decay of ϕ takes place $\phi(t) = \phi_0 e^{-t/\tau}$. We have determined τ and then in turn $\phi(t)$ by analyzing the backisomerization behavior of bulk DNMR spectra, taking into account experimental points $\phi_0 = 1$ and $\phi(t \geq t_{\mathrm{N}}) = I_{\mathrm{N}}^{cis}/I_{\mathrm{N}}$. Here t_{N} is the time of disappearance of the paranematic component of the spectrum. Within the investigated temperature interval (300 K–325 K), τ exhibits an Arrhenius-type behavior $\tau(T) = \tau_\infty e^{E_a/k_B T}$ with $\tau_\infty \approx 2 \times 10^{-7}$ s and activation energy $E_a \approx 680$ meV.

In the paranematic phase, the surface interactions-controlled order parameter is known to exhibit a radial decay profile $S(r)$ with maximal value at the surface [6]. However, on the characteristic time scale of the DNMR experiment, $\tau_{\mathrm{DNMR}} \approx \Delta\nu_{\mathrm{PN}}^{-1}$, typically a few milliseconds, the diffusion of molecules in radial direction is larger than the pore size $\langle r^2 \rangle = 4D\tau_{\mathrm{DNMR}} > R^2$ assuming conventional diffusion rate $D \approx 10^{-10}$ m^2/s [18]. The director field is thus scanned in the fast motion limit, with apparently axial profile like in the nematic phase, and the small observed paranematic splitting reflects the averaged paranematic order $S_{\mathrm{PN}} = \overline{S(r)}$.

Using the above facts, experimental *cis*-concentration profiles of the order parameters $S_{\mathrm{N}}^{trans}(\phi)$ and $S_{\mathrm{PN}}(\phi)$ were calculated for measurements performed at different temperatures and are shown in Fig. 2(a). Acquisition of $S_{\mathrm{N}}^{cis}(\phi)$ profiles with comparably low experimental error would require considerably longer signal accumulation, without the prospect to gain important additional information; therefore, it has not been performed, and in the following we denote $S_{\mathrm{N}}^{trans}(\phi)$ with $S_{\mathrm{N}}(\phi)$. The three characteristic regions of the phase diagram can clearly be discerned: the PN phase at higher values of ϕ, the N + PN coexistence for intermediate ϕ, and the re-entrance into the N phase for low ϕ. It is noteworthy that both bulk and surface order parameters remain constant in the coexistence region.

Identifying a phase coexistence behavior spanning over an extremely broad temperature interval supports the proposition that photoisomerized 7AB behaves as binary nematogen. Such a system can be theoretically modeled by combining the theories of isotropic mixing and Maier-Saupe-type nematic ordering [19]. The paranematic

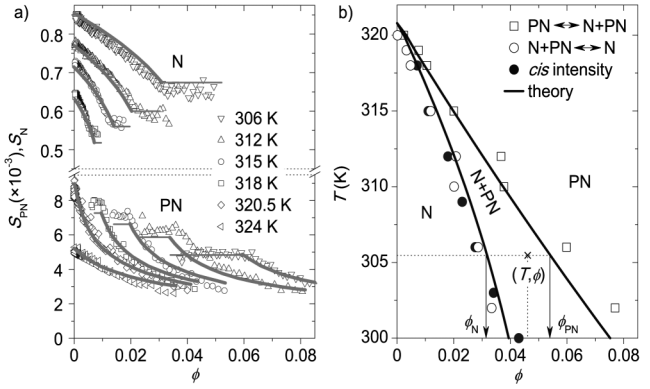

FIG. 2. (a) Experimentally determined ϕ-dependencies of the nematic $S_{\mathrm{N}}(\phi)$ and paranematic $S_{\mathrm{PN}}(\phi)$ order parameters at different temperatures. Theoretical fits are shown as thick solid lines (N and PN phases without coexistence) and thin solid lines (N + PN phase coexistence). Best fit parameters are $U_0 = 9.4 \times 10^{-3}$ eV, $U/U_0 = 6.9$, $T^* = 319$ K, $a/U_0 = 0.02$ K^{-1}, $B/U_0 = 0.18$, $E/U_0 = 0.8$, $L/U_0 = 1.1$ nm^2, and $S_0 = 0.07$. (b) Phase diagram of photoisomerized 7AB. Dotted lines are guides for the determination of boundary values ϕ_{N} and ϕ_{PN} for a given (T, ϕ) point within the N + PN coexistence region. Solid lines were calculated by disregarding the F_{PN} term, since its impact on their shape is minute due to low value of S_{PN}.

behavior at high temperatures can be accounted for by including surface contributions [12]. The full free energy F can therefore be written as a sum of

$$F_{\mathrm{mix}} = kT[\phi \ln\phi + (1-\phi)\ln(1-\phi)] + U_0\phi(1-\phi), \tag{1a}$$

$$F_{\mathrm{N}} = -\frac{U}{2}S^2(1-\phi)^2 + \left[\frac{a}{2}(T-T^*)S^2 + \frac{U}{2}S^2 - \frac{B}{3}S^3 + \frac{E}{6}S^6\right](1-\phi), \tag{1b}$$

and

$$F_{\mathrm{PN}} = \left(\frac{L}{2}\overline{\nabla S^2} - \frac{U}{2}\bar{S}^2\right)(1-\phi)^2 + \left[\frac{a}{2}(T-T^*)\bar{S}^2 + \frac{U}{2}\bar{S}^2 - GS_0\right](1-\phi). \tag{1c}$$

F_{mix} describes the change in the free energy per molecule when two species of isotropic molecules, *trans* and *cis* in our specific case, are mixed. U_0 is the Flory interaction parameter. We have approximated the Maier-Saupe binary nematic bulk free energy F_{N} and and surface free energy F_{PN} [19] by their LdG analogue. The experimental data are optimally modeled with $C = D = 0$ and non-zero S^6 term in Eq. (1b) (Ref. [20]). Here S is the nematic order parameter of *trans* molecules, U quantifies the interaction among trans molecules, and T^*, a, B and E are the classical LdG parameters. The *cis* concentration ϕ is included in the standard LdG expression by observing that the single-particle terms, i.e., entropy and surface interaction terms,

should depend linearly on the *trans* concentration $1-\phi$, whereas the inter-particle terms should scale as $(1-\phi)^2$. The terms representing nematic order of *cis* molecules are not considered in F_N and F_{PN}, an unjustified assumption as the Fig. 1(c) spectrum clearly resolves the nematic *cis*-doublet. It can however be shown that the weak orientational ordering of *cis* isomers does not significantly influence the orientational ordering of *trans* isomers, so that the former can be treated as nonmesogenic solutes. The experimentally observed strong ϕ-dependence of S_{PN} and saturation of both S_N and S_{PN} in the coexistence region reflects a substantial interplay between the surface and bulk order. This calls for inclusion of mixing (ϕ-dependent) terms in the surface free energy term [Eq. (1c)]. The averages $\overline{\nabla S^2}$ and $\bar{S}^2$ in the elastic deformation term and LdG term, respectively, are over the radial profile of the paranematic order $S(r)$. G is the surface anchoring energy and S_0 the nematic order at the surface [12]. Due to small S_0, higher order terms in $S(r)$ can be disregarded and the PN-N transition remains subcritical.

Using the above assumptions, the high-temperature paranematic solution $S_{PN}(T,\phi)$ and the low-temperature nematic solution $S_N(T,\phi)$ are obtained by separately minimizing F_{PN} and F_N with respect to S [thick solid lines in Fig. 2(a)]. However, these are proper solutions only for (T,ϕ) points at which no demixing of components, resulting in an N + PN phase coexistence, takes place. The coexistence region of the $T-\phi$ phase diagram is determined by requiring that chemical potentials of the coexisting phases match, equivalently $F'(\phi_N) = F'(\phi_{PN})$ and $F(\phi_N) - \phi_N F'(\phi_N) = F(\phi_{PN}) - \phi_{PN}F'(\phi_{PN})$ [21]. These expressions implicitly define the nematic phase boundary line $\phi_N(T)$ and paranematic phase boundary line $\phi_{PN}(T)$ shown in Fig. 2(b). Whenever ϕ is altered due to either photoisomerization or thermal backisomerization at a fixed temperature, ϕ_N and ϕ_{PN} remain constant while satisfying $\phi = \phi_N x + \phi_{PN}(1-x)$, and it is the changing volume fractions x and $1-x$ of the respective N and PN phases that compensate for the change in ϕ. This also explains why S_N and S_{PN} are invariant to isothermal changes of ϕ in the coexistence region since they solely depend on T for $\phi_{PN} \le \phi \le \phi_N$. Theoretical phase boundaries are in a good agreement with the experimental data shown in Fig. 2(b). We also note that $C = D = 0$ version of F_N [Eq. (1b)] more optimally fits the experimental points than the $C = E = 0$ version. Similar N + PN phase coexistence behavior of the nematic and paranematic order, specifically T-independent DNMR quadrupolar splitting in the biphasic region, has been found in the external magnetic-field induced bulk paranematic phase of a binary mixture of a nematogen with nonmesomorphic solute [22].

As far as orientational ordering is concerned, the system is considered to retain its state whenever the order parameter remains constant while the externally-controllable

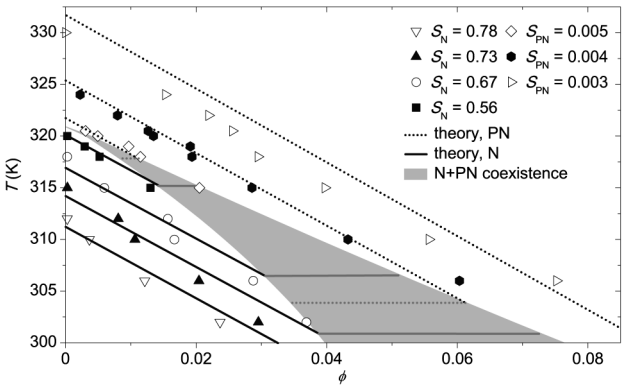

FIG. 3. Experimental (symbols) and theoretical (solid lines) isonematic and isoparanematic curves of the 7AB T-ϕ phase diagram. These curves extend as horizontal lines into the coexistence region (shaded area).

parameters T and ϕ are varied. Outside the N + PN coexistence region, the dependence of orientational order parameters on T and ϕ can be expressed in terms of effective temperature, i.e., $S_N = S_N(\tilde{T}_N)$ and $S_{PN} = S_{PN}(\tilde{T}_{PN})$, with $\tilde{T}_N(T,\phi) = T + \frac{U}{a}\phi$ and $\tilde{T}_{PN}(T,\phi) = T + (\frac{U}{a} - T^*)\phi(1-\phi)^{-1}$. The isonematic (constant S_N) and isoparanematic (constant S_{PN}) curves of the $T-\phi$ phase diagram are therefore straight lines, given by $T_N(S_N;\phi) = \tilde{T}_N(S_N) - \frac{U}{a}\phi$ and $T_{PN}(S_{PN};\phi) = \tilde{T}_{PN}(S_{PN})(1-\phi) + (T^* - \frac{U}{a})\phi$, respectively. $\tilde{T}_N(S_N)$ and $\tilde{T}_{PN}(S_{PN})$ are the respective inverse functions of $S_N(\tilde{T}_N)$ and $S_{PN} = S_{PN}(\tilde{T}_{PN})$. The linear relationship between T and ϕ was indeed confirmed experimentally (see Fig. 3). The "lyotropic" behavior of the system, i.e., the dependence of the order parameters on ϕ can therefore be described within the thermotropic phase transition model by introducing the effective temperature that linearly depends on ϕ. The above observations of N + PN phase coexistence, *cis* and *trans* component demixing, and order parameter saturation, clearly demonstrates that the behavior, characteristic of bulk binary system, is not suppressed in the nanosized environment of cylindrical pores. Since liquid phases of adjacent pores are not interconnected, one can overrule an alternative description of phase coexistence in terms of distributed transition temperatures, originating from the differences in ϕ across the sample.

In conclusion, we have shown that photoisomerized 7AB can be used as a model system for investigation of phase separation behavior of binary nematogenic mixtures in confined geometries. By dynamically controlling the populations of the two components, *trans* and *cis*, via UV-illumination, we have for the first time determined the $T-\phi$ phase diagram of a confined binary nematogen, exhibiting surface-induced paranematic to nematic phase transition with a broad intermediate phase coexistence region. The isothermal values of both the nematic and paranematic order parameters are independent of ϕ in the coexistence region, reflecting the establishment of

chemical equilibrium within individual nanosized regions. The ability to locally manipulate the nematic bulk and surface order by simultaneous control of temperature and concentration may prove important for future applications in microfluidics and micro- and nanomechanical devices.

This work was supported by the Spanish MICINN (MAT2009-14636-C03-02) and the Slovenian Research Agency (P1-0125). Any opinions, findings, and conclusions or recommendations expressed in this article are those of the authors and do not necessarily reflect the views of the National Science Foundation.

[1] G. P. Crawford and S. Žumer, in *Liquid Crystals in Complex Geometries: Formed by Polymer and Porous Networks* (Taylor & Francis, London, 1996).
[2] T. Moses and Y. R. Shen, Phys. Rev. Lett. **67**, 2033 (1991).
[3] G. S. Iannacchione, G. P. Crawford, S. Žumer, J. W. Doane, and D. Finotello, Phys. Rev. Lett. **71**, 2595 (1993).
[4] A. V. Kityk, M. Wolff, K. Knorr, D. Morineau, R. Lefort, and P. Huber, Phys. Rev. Lett. **101**, 187801 (2008).
[5] P. Sheng, Phys. Rev. A **26**, 1610 (1982).
[6] G. P. Crawford, R. J. Ondris-Crawford, J. W. Doane, and S. Žumer, Phys. Rev. E **53**, 3647 (1996).
[7] P. A. Kossyrev and G. P. Crawford, Mol. Cryst. Liq. Cryst. Sci. Technol., Sect. A **351**, 379 (2000).
[8] T. Ikeda and O. Tsutsumi, Science **268**, 1873 (1995).
[9] S. Samitsu, Y. Takanishi, and J. Yamamoto, Nature Mater. **9**, 816 (2010).
[10] X. Tong, L. Cui, and Y. Zhao, Macromolecules **37**, 3101 (2004).
[11] H. Chiu and T. Kyu, J. Chem. Phys. **103**, 7471 (1995).
[12] G. P. Crawford, R. Stannarius, and J. W. Doane, Phys. Rev. A **44**, 2558 (1991).
[13] G. P. Crawford, L. M. Steele, R. Ondris-Crawford, G. S. Iannacchione, C. J. Yeager, J. W. Doane, and D. Finotello, J. Chem. Phys. **96**, 7788 (1992).
[14] B. Zalar, O. D. Lavrentovich, H. Zeng, and D. Finotello, Phys. Rev. E **62**, 2252 (2000).
[15] G. Zimmerman, L.-Y. Chow, and U.-J. Paik, J. Am. Chem. Soc. **80**, 3528 (1958).
[16] W. R. Folks, Y. A. Reznikov, S. N. Yarmolenko, and O. D. Lavrentovich, Mol. Cryst. Liq. Cryst. Sci. Technol., Sect. A **292**, 183 (1997).
[17] T. Jin, B. Zalar, A. Lebar, M. Vilfan, S. Žumer, and D. Finotello, Eur. Phys. J. E **16**, 159 (2005).
[18] S. V. Dvinskikh, I. Furó, H. Zimmermann, and A. Maliniak, Phys. Rev. E **65**, 061701 (2002).
[19] F. Brochard, J. Jouffroy, and P. Levinson, J. Phys. (Paris) **45**, 1125 (1984).
[20] E. F. Gramsbergen, L. Longa, and W. H. de Jeu, Phys. Rep. **135**, 195 (1986).
[21] M. Kleman and O. D. Lavrentovich, in *Soft Matter Physics: An Introduction* (Springer-Verlag, New York, 2003).
[22] G. S. Attard, J. W. Emsley, S. K. Khoo, and G. R. Luckhurst, Chem. Phys. Lett. **105**, 244 (1984).